

Article

Causal Geometry

Pavel Chvykov ^{1,*}  and Erik Hoel ²

¹ Physics of Living Systems, Massachusetts Institute of Technology, Cambridge, MA, USA; pchvykov@mit.edu

² Allen Discovery Center, Tufts University, Medford, MA, USA; erik.hoel@tufts.edu

* Correspondence: pchvykov@mit.edu

Received: date; Accepted: date; Published: date

Abstract: Information geometry has offered a way to formally study the efficacy of scientific models by quantifying the impact of model parameters on the predicted effects. However, there has been little formal investigation of causation in this framework, despite causal models being a fundamental part of science and explanation. Here we introduce causal geometry, which formalizes not only how outcomes are impacted by parameters, but also how the parameters of a model can be intervened upon. Therefore we introduce a geometric version of “effective information”—a known measure of the informativeness of a causal relationship. We show that it is given by the matching between the space of effects and the space of interventions, in the form of their geometric congruence. Therefore, given a fixed intervention capability, an effective causal model is one that matches those interventions. This is a consequence of “causal emergence,” wherein macroscopic causal relationships may carry more information than “fundamental” microscopic ones. We thus argue that a coarse-grained model may, paradoxically, be more informative than the microscopic one, especially when it better matches the scale of accessible interventions—as we illustrate on toy examples.

Keywords: model selection; causality; sloppy models; information geometry; effective information; causal emergence

1. Introduction

Many complex real-world phenomena admit surprisingly simple descriptions, from the smallest of microphysics to aspects of economics [1–3]. While this is not seen as entirely coincidental, the precise reasons for this fortunate circumstance are not entirely understood [4,5]. Two complementary solutions may be sought: On the one hand, we may hypothesise that this is an objective property of nature, thereby looking for some mechanism common among complex systems that allows them to be well-described with only a few parameters [3,6]. On the other, we may guess that it is a subjective property of our perception, and then try to formalize the process by which we find useful patterns in arbitrarily complex systems [5,7,8]. In the recent years, substantial progress has been made in developing both these perspectives, grounded in Information Theory [9].

One compelling argument for the first hypothesis has been made from Information Geometry. The approach starts by associating to any given model a particular “model manifold,” whose geometric properties can tell us whether and which simplifications can be helpful [6,10]. It turns out that for many real-world models this manifold is highly anisotropic, having a hierarchical hyper-ribbon structure [11]. This property, termed “sloppiness,” indicates that only few of the many microscopic model parameters are actually important for the model predictions—thus allowing for model simplification [12,13]. While it is not yet clear how general this property is, sloppiness was empirically illustrated in a number of biochemical and physical models, and argued for on some general grounds [6,14,15]. This way sloppiness provides an explanation for how emergent simplicity may be an objective property of complex systems themselves.

The second perspective instead takes as its starting point the well-known aphorism that “all models are wrong, but some are useful” [7]. One way to see this is as a rejection of the reductionist notion that a “fundamental” microscopic description is best, while all emergent system properties are derivative from it [2,16]. Instead, if no model is seen as fundamentally correct, then we can only compare models by their efficacy in predicting and controlling a given system. In this perspective, simple descriptions may arise not from any property of the complex system itself, but from our efforts to match the system description to how we interact with it [8,9].

In particular, we may see this as the search for an optimal causal model of a system. For this, we view physical systems as sets of input-output relations, with inputs given by the experimentally doable interventions or controls, and outputs—by the effects of interest we choose to observe. Even so, reliably identifying causal relationships is often difficult, especially in complex systems [17,18]. By combining information theory and Judea Pearl’s causal calculus [19], we can rigorously quantify the amount of *Effective Information* (EI) in the causal structure of a given model [20]. Previously it has been shown that for some systems a dimension-reduced model (such as a coarse-graining) may actually be more informative in terms of EI than the full microscopic one—a phenomenon termed “Causal Emergence” [21]. Crucially, this result does not rely on an explicit preference for simplicity, but directly shows that higher-level descriptions may, paradoxically, be more informative—specifically in the sense of having more informative causal relationships [22]. This is possible because a dimension-reduced model may be less noisy and less degenerate.

In this work, we extend the Causal Emergence framework to continuous systems, and show that in that context, it is naturally related to Information Geometry and sloppy models. This leads to a novel construction, which we term Causal Geometry, where finding the causally most informative model translates to a geometric matching between our intervention capabilities and the effects on system behaviors, both expressed as distance metrics on the model’s parameter space. This framework captures precisely how the inherent properties of the system’s behavior, and their relation to its use context, both play a role in optimal model selection, thereby reconciling the two above perspectives. This comes up because on the one hand, intervention capabilities are never unlimited in their degree or fineness and perfection of control, and on the other, because the behaviors of open physical systems are never without noise. This helps to formalize how neither the “simplest” nor the most “fundamental” reductionist model may be universally seen as preferable.

In section 2 we define the EI for continuous models, which captures the amount of information in the model’s causal relationships. We illustrate it on a simple example (section 2.1), and show how restricting the set of allowed interventions may sometimes, surprisingly, make the causal model more informative. Section 3 then introduces Causal Geometry. Specifically, it relates the continuous EI to information geometry, introducing a local geometric measure of causal structure EI_g , and providing a way to find the locally most effective model for a given set of intervention capabilities, using the techniques of information geometry. We demonstrate our construction on another simple toy-model in section 4, showing how causal emergence can arise in our geometric formulation, subject to the given interventional and observational capabilities.

2. Effective Information (EI) in continuous systems

For the purposes of this work, we formalize a *causal model* as a set of input-output relations, or more precisely, a map from all possible interventions to the full description of all effects within the context of some system [22]. While the set of all hypothetically possible interventions on a given physical system is enormous and impractical to consider (involving arbitrary manipulations of every subatomic particle), the set of experimentally doable (or even considered) interventions for a given context always represent a

much smaller bounded space \mathcal{X} , which we refer to here as “intervention capabilities.” Similarly, while an intervention will lead to uncountable microscopic physical effects, the space of specific effects of interest \mathcal{Y} is much smaller, and often happens to be closely related to the intervention capabilities. All causal models by definition use some such subset of possibilities and it is common in the literature around causation to restrict the set of hypotheticals, or counterfactuals, within a causal model [23]. In this work, we will illustrate how finding the optimal causal model for a given system is about a matching between the system behavior and the intervention capabilities considered.

As the focus of this paper is on continuous systems, we consider \mathcal{X} and \mathcal{Y} to be continuous spaces, with points $x \in \mathcal{X}$ and $y \in \mathcal{Y}$. To formally discuss the causal model of our system, we make use of the $do(x)$ operator, as per Judea Pearl’s causal calculus [19]. This operator is defined for any doable intervention the experimenter is capable of either performing or modeling, allowing to assess its causal effects. This allows us to formally describe a causal model as a map

$$x \rightarrow p(y | do(x)) \quad (1)$$

where p is the probability density over effect space \mathcal{Y} resulting from “doing” the intervention x . Note that this is distinct from $p(y | x)$ in that the do operator allows us to distinguish the correlation introduced by the causal relation $x \rightarrow y$ from one due to a common cause $a \rightarrow \{x, y\}$.

The notion of causality is then formalized as a counterfactual: how does the effect of $do(x)$ differ from the effect of not doing x ? This latter “null effect” may be formally described by averaging together the effects of all considered intervention capabilities \mathcal{X} , giving the total “effect distribution”:

$$E_D(y) = \langle p(y | do(x)) \rangle_{x \in \mathcal{X}} \quad (2)$$

This way to know precisely which effects does $do(x)$ cause, we can compare $E_D(y)$ to $p(y | do(x))$. The distinguishability between these distributions may be captured with the Kullback-Leibler Divergence $D_{KL}[p(y | do(x)) \parallel E_D(y)]$, giving us the amount of information associated with the application of an individual $do(x)$ intervention [21,24].

Averaging over all accessible interventions gives the information of the system’s entire causal structure, termed the total “effective information”:

$$EI = \langle D_{KL}[p(y | do(x)) \parallel E_D(y)] \rangle_{x \in \mathcal{X}} \quad (3)$$

Discrete versions of this effective information have been explored in Boolean networks [21] and graphs [25]. Note that the definition of EI here is identical to the mutual information between the uniform distribution over interventions $I_D(x) = \text{const}$ and the resulting distribution over effects $E_D(y)$, so that: $EI = \mathcal{I}(I_D; E_D)$ [20,22].

We proceed to illustrate on a simple example how the EI varies across families of simple physical systems. As such, we show how it may be used to select the systems that are in some sense “best controllable,” in that they best associate unique effects to unique interventions [26]. Additionally, this example will help us illustrate how the EI may sometimes allow us to identify a coarse-grained system description that is more informative than the full microscopic one—thus illustrating Causal Emergence [22].

2.1. Toy example: dimmer switch

Consider a continuous dimmer-switch controlling a light-bulb, but with an arbitrary non-linear function $y = f(\theta)$, a “dimmer profile,” mapping from the switch setting $\theta \in \Theta = [0, 1]$ to the light-bulb brightness $y \in \mathcal{Y} = [0, 1]$ (Figure 1a). To quantify information about causation in continuous systems,

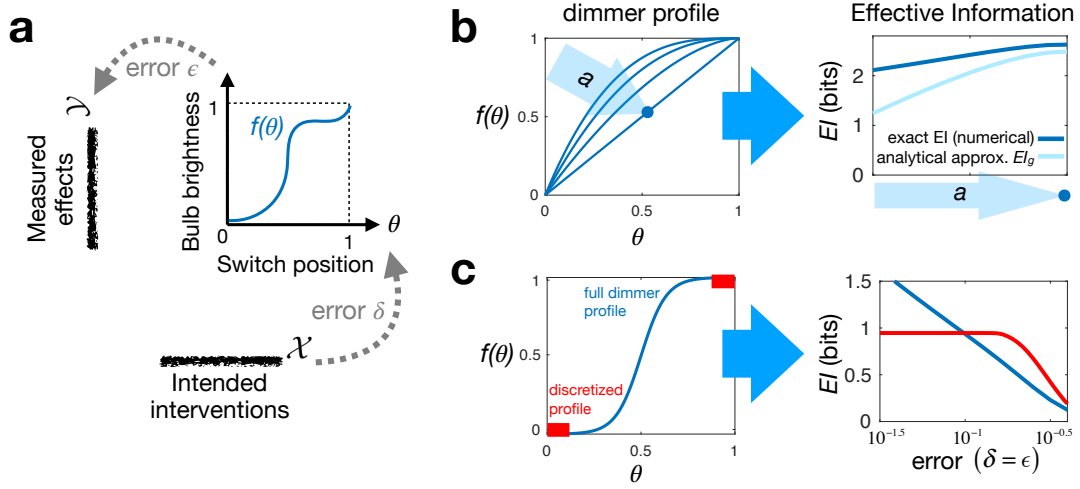


Figure 1. Illustrating continuous Effective Information (EI) on a simple toy system. (a) shows the system construction: a dimmer switch with a particular “dimmer profile” $f(\theta)$. We can intervene on it by setting the switch $\theta \in (0, 1)$ up to error tolerance δ , while effects are similarly measured with error ϵ . (b) shows that for uniform errors $\epsilon = \delta = 0.03$, out of the family of dimmer profiles parametrized by a (left), the linear profile gives the “best control,” i.e., has the highest EI (where dark blue—numerical EI calculation and light blue—approximation in Eq. 4). (c) illustrates how for two other dimmer profiles (left), increasing error tolerances $\epsilon = \delta$ influences the EI (right, calculated numerically). The profile in red represents a discretized binary switch—which emerges if we restrict the interventions on the blue dimmer profile to only use “ends of run.” Crucially, such coarse-graining allows for an *improved* control of the light (higher EI) when errors are sufficiently large.

we must carefully account for noise and errors in our inputs and outputs—else, infinite precision leads to infinite information. This is an issue for the application of all mutual information measures or their derivatives in deterministic continuous systems. Realistically, in operating a dimmer-switch, any user will have certain “intervention error” on setting its value, as well as “effect error,” which can come either from intrinsic system noise, or from extrinsic measurement error. To encode the effect error, we can replace the deterministic mapping $\theta \rightarrow y = f(\theta)$ with a probabilistic one $\theta \rightarrow p(y | do(\theta)) = \mathcal{N}_y(f(\theta), \epsilon^2)$ —the normal distribution centered on $f(\theta)$ and with standard deviation ϵ . While we could incorporate intervention error of setting θ into this probability distribution as well, it is instructive for latter discussion and generality to keep it separate. The intervention error is thus similarly encoded by introducing a probabilistic mapping from the “do”-able interventions $x \in \mathcal{X} = [0, 1]$ to the physical switch settings with some error δ , as $x \rightarrow q(\theta | do(x)) = \mathcal{N}_\theta(x, \delta^2)$. Here we can think of the interventions $x \in \mathcal{X}$ as the “intended” switch settings, as in practice we cannot set the switch position with infinite precision.

With this setup, we can now use Eq. 3 to explicitly compute an EI for different dimmer profiles $f(\theta)$ and see which is causally most informative (has most distinguishable effects). To do this analytically for arbitrary $f(\theta)$, we must take the approximation that δ and ϵ are small compared to 1 (the range of interventions and effects), and compared to the scale of curvature of $f(\theta)$ (such that $\epsilon f''(\theta) \ll f'(\theta)^2$). In this limit, we have (for derivation, see setup in Eq. 6 below and Appendix A.1):

$$EI \simeq -\frac{1}{2} \int d\theta \log \left[2\pi e \left(\left(\frac{\epsilon}{f'(\theta)} \right)^2 + \delta^2 \right) \right], \quad (4)$$

which echoes the form of the expression for entropy of a normal distribution. From this, we see variationally that, given the fixed end-points $f(0) = 0$ and $f(1) = 1$, EI is maximized iff $f'(\theta) = 1$: a uniformly linear dimmer switch. We can check this numerically by computing the exact EI for several different choices of $f(\theta)$ —Figure 1b.

A slightly more interesting version of this example is when our detector (eyes) perceive light brightness on a log, rather than linear, scale (Weber-Fechner law, [27]), in which case the effect error will be non-uniform: $\epsilon(y) \propto y$. If this error is bound to be sufficiently small everywhere, Eq. 4 still holds, replacing only $\epsilon \rightarrow \epsilon(y) \propto y = f(\theta)$. Again, we can variationally show that here EI is maximal iff $f(\theta)/f'(\theta)$ is constant (up to fluctuations of magnitude $O[\delta/\epsilon]$), giving the optimal dimming profile $f(\theta) = (e^{\theta/r} - 1)/(e^{1/r} - 1)$, with some constant $r \ll \delta/\epsilon$. In reality, the lighting industry produces switches with many dimming profiles that depend on the application [28]—so our approach can be seen as a principled way to optimize this choice.

Interestingly, restricting the accessible interventions can sometimes increase the amount of effective information if it increases the distinguishability, and therefore informativeness, of interventions. This is a form of causal emergence, wherein a higher-level (coarsened) macroscopic model emerges as the more informative system description for modeling causation [22]. To give a particular example here, we compare the continuous dimmer profile shown in Figure 1c (left, blue) to its discrete restriction (left, red)—which corresponds to a simple binary switch. When the intervention and effect errors $\delta = \epsilon$ are small, the continuous switch gives more control opportunities, and is thus preferable—its EI is larger than the 1 bit for the discrete switch. However, as we increase the errors, we see a crossover in the two EI values. In this regime, the errors are so large that the intermediate switch positions of the continuous profile become essentially useless, and are “distracting” from the more useful endpoint settings. Formally, such causal emergence arises due to the averaging over the set of all interventions in Eq. 3. Practically, it captures the intuition that building good causal models, as well as designing useful devices, involves isolating only the most powerful control parameters out of all possible degrees of freedom [26].

3. Causal Geometry

Taking inspiration from information geometry, we can construct a more intuitive geometric expression for the EI [13]. For studying causal structures of models, this “geometric EI ” we introduce may be viewed as a supplement to the usual EI in Eq. 3. While the geometric EI corresponds with EI in a particular limit, we suggest that it remains useful more generally as an alternative metric of causal efficacy: it captures a causal model’s informativeness like the EI does, but in a way that is local in a system’s parameter space. In this way, it frames causality not as a global counter-factual (comparing an intervention to all other interventions) [19], but as a local neighborhood counter-factual (comparing an intervention to nearby interventions). On the flip side, our construct provides a novel formulation of Information Geometry that allows it to explicitly account for causal relations of a model. Moreover, we argue that this is necessary for formal consistency when working with the Fisher information matrix eigenvalues (namely, their covariant formulation, see section 3.2) [29]. This suggests that model reduction based on these eigenvalues may not be made fully rigorous without explicitly accounting for causal relations in the model.

3.1. Construction

Section 2 described a causal model as a set of input-output relations between interventions \mathcal{X} and effects \mathcal{Y} . Here we investigate the relationship of such causal model with the space of parameters Θ that describe the underlying physical system. While these parameters need not necessarily have any direct physical meaning themselves, they are meant to give some abstract internal representation of the system—i.e., they mediate the mapping between interventions and effects. For example, while the notion

of energy is merely an abstract concept, it provides a useful model to mediate between interventions such as “tuning on the stove” and effects like “boiling water.” The goal of our construction here is to compare how well different physical models capture the causal structure of a system.

As we are focusing on continuous systems, we assume that our parameter space Θ forms a smooth d -dimensional manifold, with parameters θ_μ indexed by $\mu, \nu \in \{1, 2, \dots, d\}$. Each accessible intervention $x \in \mathcal{X}$ then maps to some probability distribution over parameters $x \rightarrow q(\theta | x)$, and each parameter in turn maps to a distribution over the observed effects $\theta \rightarrow p(y | \theta)$. To understand the role of various parameters θ_μ , we can ask how much the effects change as we perturb from some set of parameters in some direction: from θ to $\theta + d\theta$. Using the Kullback-Leibler divergence, and expanding it to leading order in $d\theta$, we get:

$$D_{KL}[p(y|\theta) \parallel p(y|\theta + d\theta)] \simeq g_{\mu\nu}(\theta) d\theta_\mu d\theta_\nu \quad (5)$$

where summation over repeated indices is implied. This defines the Fisher Information Metric $g_{\mu\nu}(\theta) = -\langle \partial_\mu \partial_\nu \log p(y|\theta) \rangle_{p(y|\theta)}$ with $\partial_\mu \equiv \frac{\partial}{\partial \theta_\mu}$. This introduces a distance metric on the parameter space Θ , turning it into a Riemannian manifold which we term the “effect manifold” \mathcal{M}_E (this is usually called simply the “model manifold” in the literature, but here we want to distinguish it from the “intervention manifold,” introduced below). More precisely, it is usually defined as $\mathcal{M}_E \equiv \{p(y | \theta)\}_{\theta \in \Theta}$ —the collection of all the effect distributions, or the image of the parameter space Θ under the model mapping, with Eq. 5 being the natural distance metric on this space [6,10,14].

Just as the mapping to effects defines the effect manifold \mathcal{M}_E , we can similarly construct an “intervention manifold” \mathcal{M}_I . For this, we use Bayes’ rule to invert the mapping from interventions to parameters $x \rightarrow q(\theta | x)$, thus giving $\theta \rightarrow \tilde{q}(x | \theta)$ —the probability that a given parameter point θ was “activated” by an intervention x . The intervention manifold is thus defined as $\mathcal{M}_I \equiv \{\tilde{q}(x | \theta)\}_{\theta \in \Theta}$, with the corresponding Fisher Information Metric $h_{\mu\nu}$ giving the distances on this space. With this, we can now summarize our construction:

$$\begin{aligned} &\text{interventions } x \in \mathcal{X}, \text{ parameters } \theta \in \Theta, \text{ effects } y \in \mathcal{Y} \\ &x \rightarrow q(\theta | x), \quad \theta \rightarrow p(y | \theta) \\ &\text{effect manifold } \mathcal{M}_E \equiv \{p(y | \theta)\}_{\theta \in \Theta} \quad \text{with metric } g_{\mu\nu}(\theta) = - \int dy p(y | \theta) \partial_\mu \partial_\nu \ln p(y | \theta) \\ &\text{intervention manifold } \mathcal{M}_I \equiv \{\tilde{q}(x | \theta)\}_{\theta \in \Theta} \quad \text{with metric } h_{\mu\nu}(\theta) = - \int dx \tilde{q}(x | \theta) \partial_\mu \partial_\nu \ln \tilde{q}(x | \theta) \\ &\text{where } \tilde{q}(x | \theta) \equiv \frac{q(\theta | x)}{\int dx q(\theta | x)} \quad \text{and } \partial_\mu \equiv \frac{\partial}{\partial \theta_\mu} \text{ with } \mu, \nu \in \{1, 2, \dots, d\} \end{aligned} \quad (6)$$

Note that for Bayesian inversion in the last line, we used a uniform prior over the intervention space $I_D(x) = \text{const}$, which amounts to assuming that statistically, interventions are uniformly distributed over the entire considered space \mathcal{X} [22].

The natural point-wise correspondence between the two manifolds $\mathcal{M}_E \leftrightarrow \mathcal{M}_I : p(y | \theta) \leftrightarrow \tilde{q}(x | \theta)$ then allows for a local comparison between the two geometries. Alternatively, we may simply think of the parameter space Θ with two separate distance metrics on it, effect metric $g(\theta)$ and intervention metric $h(\theta)$. With this setup, we can now define our “geometric” effective information:

$$EI_g = \log \left[\frac{V_I}{(2\pi e)^{d/2}} \right] - \langle l(\theta) \rangle_I \quad (7)$$

$$\text{with } l(\theta) = \frac{1}{2} \log \det \left(\mathbb{1} + g(\theta)^{-1} h(\theta) \right) \quad (8)$$

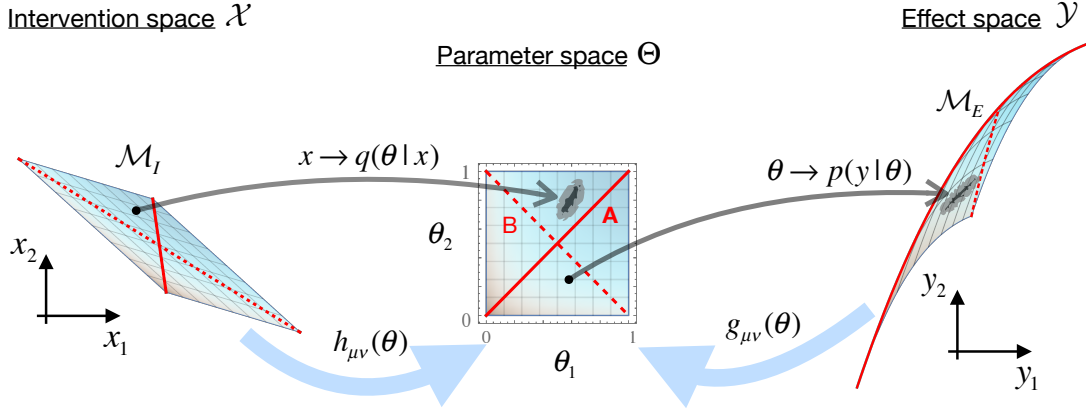


Figure 2. An illustration of the Causal Geometry construction in Eq. 6. The parameter space Θ of our model gets two distinct geometric structures: the effect metric $g_{\mu\nu}(\theta)$ and the intervention metric $h_{\mu\nu}(\theta)$. Here, a model is seen as a map that associates to each set of parameters θ , some distribution of possible measured effects y (right). As parameters θ may involve arbitrary abstractions and thus need not be directly controllable, we similarly associate them to practically doable interventions x (left). This way, our system description in terms of θ “mediates” between the interventions and resulting effects in the causal model.

Here V_I is the volume of the intervention manifold \mathcal{M}_I , which can be computed as $V_I = \int d^d\theta \sqrt{\det h}$. It quantifies the effective number of distinct interventions we can do, and so the first term in Eq. 7 gives the maximal possible amount of information about causation our model could have, if all interventions perfectly translated to effects. The second term then discounts this number according to how poorly the interventions actually overlap with effects: geometrically, the expression in Eq. 8 quantifies the degree of matching between the metrics g and h at the point θ (here $\mathbb{1}$ stands for the identity matrix). This way, the loss term $l(\theta)$ can be interpreted as a measure of “local mismatch” between interventions and effects at θ , quantifying how much information about causation is lost by our modeling choice. The average is then taken according to the intervention metric as: $\langle l(\theta) \rangle_I \equiv \frac{1}{V_I} \int d^d\theta \sqrt{\det h} l(\theta)$. Note that the expression in Eq. 7 is identical to the approximation in Eq. 4 for the setup in that example.

In Appendix A.2 we show that this expression for EI_g in Eq. 7 can be derived as the approximation of the exact EI in Eq. 3 when both the mappings are close to deterministic: $p(y|\theta) = \mathcal{N}_y(f(\theta), \epsilon^2)$ and $\tilde{q}(x|\theta) = \mathcal{N}_x(F(\theta), \delta^2)$, for some functions $f: \Theta \rightarrow \mathcal{Y}$ and $F: \Theta \rightarrow \mathcal{X}$, with small errors ϵ and δ (which may be anisotropic and nonuniform). Outside of this regime, the EI and EI_g can differ. For instance, while EI is positive by definition, EI_g can easily become negative, especially if g is degenerate anywhere on the manifold. Second, while EI captures the informativeness and therefore effectiveness of a causal model globally, EI_g , and more specifically the landscape $l(\theta)$, can show us which local sectors of the parameter space are most and least causally effective. Finally, the global nature of the computation for the exact EI quickly makes it intractable, even numerically, for many continuous systems due to proliferation of high-dimensional probability distributions—making EI_g the more practical choice in those settings.

3.2. Relation to Sloppiness

“Sloppiness” is the property empirically observed in many real-world models, when the eigenvalues of the Fisher information matrix $g_{\mu\nu}$ take on a hierarchy of vastly varying values [6,11,14]. As such, parameter variations in the directions corresponding to the smallest eigenvalues will have negligible impact on the effects [14]. This leads to the hypothesis that we may effectively simplify our model by projecting out such directions, with little loss for the model’s descriptive power [12,13].

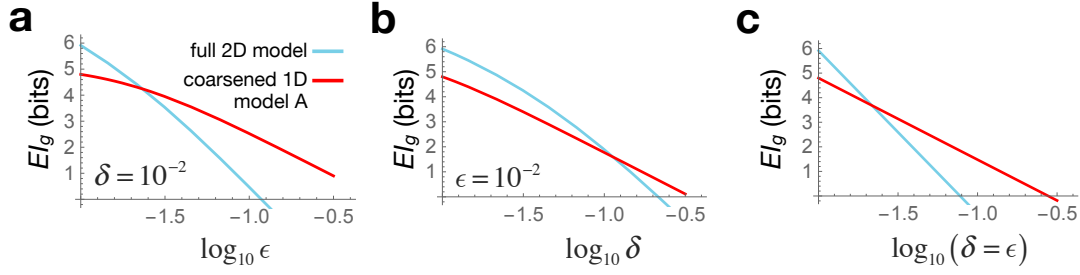


Figure 3. Causal emergence from increasing errors for the toy-model in section 4. In all panels, blue line shows the EI_g for the full 2D model, while red—for the 1D sub-manifold A shown in Figure 2 (solid red line). In (a) we vary the effect error ϵ at fixed intervention error $\delta = 10^{-2}$, (b) varies intervention error δ at fixed effect error $\epsilon = 10^{-2}$, and (c) varies both together $\delta = \epsilon$. In each case we see a cross-over where, with no change in system behavior, the coarse-grained 1D model becomes causally more informative when our intervention or effect errors become large.

The trouble with this approach is that the components of the matrix $g_{\mu\nu}$, and hence its eigenvalues, depend on the particular choice of θ -coordinates on the effect manifold \mathcal{M}_E [6,29]. Since the parameters Θ represent some conceptual abstraction of the physical system, they constitute an arbitrary choice. This means that for a given point of \mathcal{M}_E labeled by θ , we can always choose some coordinates in which locally $g(\theta) = \mathbb{1}$ (an identity matrix), thus apparently breaking the above sloppiness structure. This issue is avoided in the literature by relying on the coordinate-independent global properties of \mathcal{M}_E , namely its boundary structure [12].

Here we show that by explicitly considering intervention capabilities, we can construct a local, but still coordinate-independent sloppiness metric. This becomes possible since interventions give a second independent distance metric on Θ [29]. The matrix product $g^{-1}h$ appearing in Eq. 8 is then a linear transformation, and thus its eigenvalues are coordinate-independent. This way, to evaluate how sloppy a given causal model is, we suggest that it is more appropriate to study the eigenvalues of $h^{-1}g$ instead of those of g as is usually done [6]. If we then want to identify the directions in parameter space that are locally least informative at a point θ , we first need to re-express the metric g in terms of the coordinates for which $h(\theta) = \mathbb{1}$ locally, and then find the appropriate eigenvectors in these new coordinates.

From this perspective, we see that the usual discussion of sloppiness, which does not study interventions explicitly [6], may be said to implicitly assume that the intervention metric $h(\theta) \propto \mathbb{1}$, meaning that all model parameters directly correspond to physically doable interventions. Moreover, this requires that with respect to the given coordinate choice, each parameter can be intervened upon with equal uniform precision—which fixes the particular choice of coordinates on the parameter-space. As such, the coordinate-specific eigenvalues $\lambda_g(\theta)$ of the effect metric $g(\theta)$ studied in information geometry, become physically meaningful in this special coordinate frame. In particular, our expression for the local mismatch in Eq. 8 can here be expressed in terms of these eigenvalues as $l(\theta) = \frac{1}{2} \sum_{\lambda} \log(1 + 1/\lambda_g(\theta))$. Thus, locally the directions with the smallest λ_g account for the largest contribution to the mismatch l . This recovers the standard intuition of sloppiness: we can best improve our model’s descriptive efficacy by projecting out the smallest- λ_g directions [12,30]. By seeing how this result arises in our framework, we thus point out that it formally relies on the implicit assumption of uniform intervention capabilities over all model parameters.

4. 2-dimensional example

In order to illustrate our causal geometry framework explicitly and show how higher-level descriptions can emerge within it, we use a simple toy-model (based on example considered in [12,13]).

Imagine an experimenter has a mixed population of two non-interacting bacterial species that they are treating with two different antibiotics. The experimenter's measurements cannot distinguish between the bacteria, and so they are monitoring only the total population size over time $y(t) = e^{-\theta_1 t} + e^{-\theta_2 t}$, where $\{\theta_1, \theta_2\} \in [0, 1]$ are the death rates of the two individual species. These death rates are determined by the two antibiotic concentrations the experimenter treats the system with $\{x_1, x_2\}$, which are the possible interventions here. In the simplest case each antibiotic will influence both species via some linear transformation A , such that $\theta_\mu = \sum_i A_{\mu i} x_i$.

This setup allows us to flesh-out the causal geometry construction and illustrate causal emergence here. Our main question is, when is this system best modeled microscopically, as the two independent species, and when it behaves more like a single homogeneous population, or something else [31]? To identify when higher-scale models are more informative for the experimenter, we will calculate the geometric EL_g from Eq. 7 for the full 2D model described above, and then compare it to two separate 1D coarse-grained model descriptions, shown by the two red 1D sub-manifolds of the parameter space in Figure 2.

We first specify the quantities for the construction in Eq. 6. Our interventions x , having some uniform error tolerance δ , map to normal distributions over parameters θ as: $x \rightarrow q(\theta | x) = \mathcal{N}_\theta(Ax, A A^T \delta^2)$, giving the Bayesian inverse probability $\bar{q}(x | \theta) = \mathcal{N}_x(A^{-1}\theta, \delta^2)$, and hence the intervention metric $h_{\mu\nu} = \sum_i (A^{-1})_{i\mu} (A^{-1})_{i\nu} / \delta^2$. The effect space y is constructed by measuring population size at several time-points, spaced out at intervals Δt , such that the components of y are given by $y_n = y(n \Delta t) = e^{-n \Delta t \theta_1} + e^{-n \Delta t \theta_2}$, with $n \in \{1, 2, \dots, N\}$ and error ϵ on each measurement. Thus we have $\theta \rightarrow p(y | \theta) = \mathcal{N}_y(\{y_n\}, \epsilon^2)$, and effect metric $g_{\mu\nu} = \sum_n \partial_\mu y_n \partial_\nu y_n / \epsilon^2$. Figure 2 shows these mapping with $N = 2$ for visual clarity, and we use $N = 3$ for the EL_g calculations below, but all the qualitative behaviors remain the same for larger N . Figure 3 shows the resulting geometric EL_g (blue curves), computed via Eq. 7 for varying values of the error tolerances ϵ and δ .

We can similarly find the EL_g for any sub-manifold of our parameter space, which would lead to a coarse-grained causal model, with a correspondingly lower-dimensional space of intervention capabilities. To do this, we identify the pull-back of the two metrics in the full parameter space, to the embedded sub-manifold, as follows. We define a 1D submanifold of Θ as a parametric curve $(\theta_1, \theta_2) = (s_1(\sigma), s_2(\sigma))$ with the parameter σ . The pull-back effect metric on this 1D space with respect to σ will be the scalar $\hat{g}(\sigma) = \sum_{\mu, \nu} s'_\mu(\sigma) s'_\nu(\sigma) g_{\mu\nu}(s_1(\sigma), s_2(\sigma))$, and similarly for intervention metric $\hat{h}(\sigma)$. For the 1D submanifold depicted by the solid red line in Figure 2, the resulting EL_g is plotted in red in Figure 3.

The crossover seen in Figure 3 thus illustrates causal emergence: for larger error values, the coarse-grained 1D description turns out to be more informative than the full 2D model. Since this coarse-graining corresponds to the case where the two bacterial species are seen as identical $\theta_1 = \theta_2$, we can say that at large errors our bacterial colony is better modeled as a single homogeneous population. Crucially, this arises not from any change in system behavior, but merely from how we interact with it: either from what interventions we impart, or from which effects we measure. Note also that when both the intervention and effect errors are scaled together $\delta \propto \epsilon$, we see analytically from Eq. 8 that $l(\theta)$ is constant, and so

$$EL_g \sim \log V_I \sim -d \log \delta \quad (9)$$

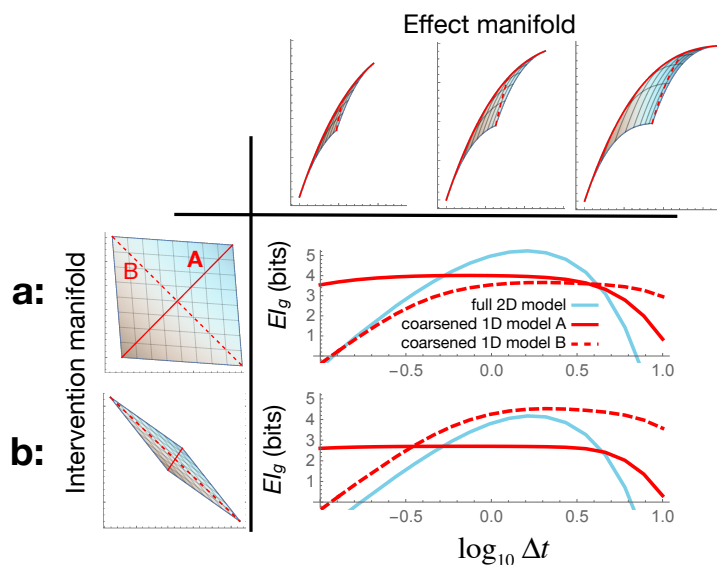


Figure 4. Optimal model choice depends on both, the effects we choose to measure and the intervention capabilities we have. Horizontally, we vary the time-scale Δt on which we measure the bacterial population dynamics in our toy-model (section 4): top row shows how this changes the shape of our effect manifold. (a) shows the results when our intervention capabilities are nearly in direct correspondence with the parameters θ . Here, the EI_g plot shows that varying Δt takes us through three regimes: with submanifold A as the optimal model at early times, the full 2D model optimal at intermediate times, and submanifold B most informative at late times. (b) shows that this entire picture changes for a different set of intervention capabilities—illustrating that appropriate model choice depends as much on the interventions as on the effects.

(Figure 3c). This indicates that, quite generally, we expect to see crossovers between geometric EI s of models with different d as we scale errors, with low-dimensional models being preferred at large noise. Since noise is ubiquitous in all real-world complex systems, this argument suggests why reductionist microscopic descriptions are rarely optimal from the perspective of informative interventions.

By carrying out similar calculations, in Figure 4 we explore how the optimal model choice depends on the time-scales we care about for the population dynamics (effects), and the antibiotics we are using (interventions), all at fixed errors ϵ , δ . When the two antibiotics control the two bacterial species almost independently ($A \sim 1$, Figure 4a), we can identify three distinct regimes in the EI_g plot as we tune the measurement time-scale Δt along the x -axis. If we only care about the population's initial response to the treatment at early times, then we get a higher EI_g by modeling our colony as a single bacterial species. For intermediate times, the full 2D model has the higher EI_g , showing that in this regime modeling both species independently is preferred. Finally, at late times, most of the population is dead, and the biggest remaining effect identifies how dissimilar their death rates were—the coarse-grained model given by the dashed red submanifold in Figure 2 ($\theta_2 = 1 - \theta_1$) turns out to be more informative. In this regime, rather than viewing the population as either one or two independent bacterial species, we may think of it as a tightly coupled ecosystem of two competing species. Interestingly, such apparent coupling emerges here not from the underlying system dynamics, but from the optimal choice of coarse-grained description for the given effects of interest.

For a different set of intervention capabilities, where the antibiotics affect both species in a more interrelated way, with $A = \begin{pmatrix} 1 & 0.8 \\ 0.7 & 1 \end{pmatrix}$, this entire picture changes (Figure 4b). In particular, we get the

scenario where the “fundamental” two-species model is never useful, and the unintuitive “two competing species” description is actually optimal at most time-scales. Note also that in all cases, for very long and very short times Δt , the geometric El_g drops below 0. While in this regime the agreement with exact El breaks down $El_g \neq El$, it is also sensible to interpret these points as the limits of that causal model’s usefulness. Even so, as seen in Figure 4, some coarse-graining of the model may still be effective beyond these limits.

5. Discussion

The world appears to agents and experimenters as having a certain scale and boundaries. For instance, solid objects are made of many loosely-connected atoms, yet in our everyday experience we invariably view them as single units. While this may be intuitively understood in terms of dictates of compression and memory storage [32], this work begins to formalize precisely how such coarse-grained modeling choice may be the correct (causally optimal) one. This is particularly true for a given set of intervention capabilities. In particular, we frame model selection as a geometric “matching” in information space of the causal model to accessible interventions.

Intriguingly, this suggests that the correct choice of scientific modeling may not be merely a function of the correct understanding of the system, but also of the context that system is being used in or the capabilities of the experimenters. Thus, for example, if the forces we used to handle solid objects were far larger than inter-atomic attraction holding them together, then viewing objects as single units would no longer be a good model. This echoes one of the main ideas in “embodied cognition” for AI and psychology, which posits that in order for an agent to build accurate models of reality, it needs the ability to actively intervene on the world, not merely observe it [33].

The Causal Geometry we introduce here is a natural extension of the Information Geometry framework [6,10], but now explicitly accounting for the causal structure of model construction. In our proposed formalism, a given model becomes associated to two distinct Riemannian manifolds, along with a mapping between them, one capturing the role of interventions, and the other—of the effects. The relative geometric matching between these two manifolds locally tells us about how causally informative the present model is, and what coarse-grainings may lead to a local improvement.

In this structure, the colloquial notion of model “sectors” (especially used in field theories to refer to various field content [34]) becomes associated to literal sectors of the manifolds, with their local geometries specifying the optimal or emergent descriptions of that sector. Such examples also highlight the importance of having a local way to quantify model optimality, as globally the manifold may have complex and piecewise structure not amenable to simplification. While both traditional El [22] and information-geometric model-reduction [12] depend on the global model behavior over the entire span of possible interventions, the geometric El_g introduced here is local to each point in parameter space. We can further speculate that fundamentally, the geometric matching in El_g may provide a novel way to quantify causality locally, where the counter-factual comparison is considered relative to the local neighborhood of interventions, rather than to all globally accessible ones [19].

We hope that Causal Geometry can contribute to further development in both, formal principled methods for optimal model building in complex systems, as well as an abstract understanding of what it means to develop informative scientific theories.

Author Contributions: Conceptualization, Pavel Chvykov and Erik Hoel; Formal analysis, Pavel Chvykov; Supervision, Erik Hoel; Visualization, Pavel Chvykov; Writing – original draft, Pavel Chvykov; Writing – review & editing, Erik Hoel.

Funding: E.H. was funded by Army Research Office Grant W911NF2010243, and P.C. by ARO W911NF1810101, and the James S. McDonnell Foundation Scholar Grant 220020476.

Acknowledgments: Thanks Mark Transtrum for helpful discussions throughout the work on the manuscript, as well as review of the final draft; Mikhail Tikhonov for inspiration at the early stages of the project; and Thomas Berrueta for great comments on the final draft.

Conflicts of Interest: The authors declare no conflict of interest.

Appendix A. Deriving geometric EI

Here we will derive the expression for EI_g in Eq. 7, and equivalently in Eq. 4. We start from the definition of EI in Eq. 3 and use the near-deterministic model approximation discussed in the main text, and below. In section A.1, we go through the detailed derivation for the 1D case, and then in section A.2 overview the steps needed to generalize it to higher dimensions.

Appendix A.1. One-dimensional case

As mentioned in the main text, the expression for EI_g presented here only approximates the exact EI when the mappings from interventions $x \in \mathcal{X}$ to parameters $\theta \in \Theta$ and to effects $y \in \mathcal{Y}$, are both nearly-deterministic. Explicitly, this means that we can express the probability distributions as Gaussians with small variances. Note that the variance can be different at different points, and in multi-dimensional case, may be anisotropic—as long as it remains sufficiently small everywhere (to be clarified later). This way, we can specify the concrete expression for the construct in Eq. 6:

$$\begin{aligned}
 &\text{interventions } x \in \mathcal{X}, \text{ parameters } \theta \in \Theta, \text{ effects } y \in \mathcal{Y} \\
 &x \rightarrow q(\theta | x), \quad \text{such that } \tilde{q}(x | \theta) \equiv \frac{q(\theta | x)}{\int dx q(\theta | x)} = \mathcal{N}_x(F(\theta), \delta^2) \\
 &\theta \rightarrow p(y | \theta) = \mathcal{N}_y(f(\theta), \epsilon^2) \\
 &g(\theta) = (f'(\theta)/\epsilon)^2 \quad \text{effect metric} \\
 &h(\theta) = (F'(\theta)/\delta)^2 \quad \text{intervention metric}
 \end{aligned} \tag{A1}$$

Note that in 1D, the metrics g and h become scalars, and $\mathcal{N}_x(F(\theta), \delta^2)$ denotes a Gaussian distribution in x , centered on $F(\theta)$ and with standard deviation δ . Also, we defined $F(\theta)$ and intervention errors δ as above, giving that $q(\theta | x) = \mathcal{N}_\theta\left(F^{-1}(x), \left(\frac{\delta}{F^{-1}'(x)}\right)^2\right)$ —merely for convenience of notation later (as δ may depend on x). As such, we also assume $F(\theta)$ and $f(\theta)$ to be invertible.

We begin with the definition of EI from Eq. 3, for which we must first calculate the distribution $P(y | x) \equiv \int d\theta p(y | \theta) q(\theta | x)$:

$$P(y | x) = \int d\theta \underbrace{\frac{1}{\sqrt{2\pi}\epsilon} e^{-\frac{(y-f(\theta))^2}{2\epsilon^2}}}_{p(y|\theta)} \times \underbrace{\frac{F'(F^{-1}(x))}{\sqrt{2\pi}\delta} e^{-\frac{(x-F(\theta))^2}{2\delta^2}}}_{q(\theta|x)} \tag{A2}$$

We can evaluate this Gaussian integral in the limit of small ϵ and δ . Let us understand precisely how small these must be.

To work with the above integral, δ must be small enough that both $\tilde{q}(x | \theta)$ and $q(\theta | y)$ are Gaussian. For this, the 2nd order term in the Taylor expansion $F(\theta) = F(\theta_x) + (\theta - \theta_x)F'(\theta_x) + \frac{1}{2}(\theta - \theta_x)^2F''(\theta_x) + \dots$ around $\theta_x \equiv F^{-1}(x)$ must be negligible in all regions with substantial probability, giving the asymptotic assumption: $\frac{1}{2}(\theta - \theta_x)^2F''(\theta_x) \ll (\theta - \theta_x)F'(\theta_x)$. We can check that in this case, plugging this expansion back into $\tilde{q}(x | \theta)$ from Eq. A1, we get now a Gaussian in θ : $\exp\left[-\frac{(\theta - \theta_x)^2 F'(\theta_x)^2}{2\delta^2}\right]$ as desired. This then shows us that we expect θ to typically be within $O[\delta/F'(\theta_x)]$ of θ_x , i.e., $(\theta - \theta_x) \sim O[\delta/F'(\theta_x)]$. This

allows us to write the above asymptotic condition as $F''(\theta) \delta \ll F'(\theta)^2$ for all θ . The exact same argument goes for the effect distribution $p(y | \theta)$, and similarly gives the condition $f''(\theta) \epsilon \ll f'(\theta)^2$. As long as these two conditions hold for all θ , we can allow $\delta = \delta(x)$ and $\epsilon = \epsilon(y)$ to vary arbitrarily.

In this limit, the integration of the expression in Eq. A2 is straightforward to carry out, giving another Gaussian:

$$P(y | x) = \frac{1}{f'(\theta_y) \sqrt{2\pi \sigma^2(\theta_x, \theta_y)}} e^{-\frac{(\theta_x - \theta_y)^2}{2\sigma^2(\theta_x, \theta_y)}}$$

$$\text{with } \sigma^2(\theta_x, \theta_y) \equiv \left(\frac{\epsilon}{f'(\theta_y)} \right)^2 + \left(\frac{\delta}{F'(\theta_x)} \right)^2 = \frac{1}{g(\theta_y)} + \frac{1}{h(\theta_x)} \quad (\text{A3})$$

where $\theta_y \equiv f^{-1}(y)$ and $\theta_x \equiv F^{-1}(x)$, and we used the expressions for the two metrics in Eq. A1. Averaging this over the interventions, and using the fact that $\sigma \sim O[\epsilon, \delta]$ —small, we can then find the effect distribution:

$$E_D(y) = \langle P(y | x) \rangle_{I_D(x)} = \int \frac{dx}{L} P(y | x) = \frac{F'(\theta_y)}{L f'(\theta_y)} \quad (\text{A4})$$

where L is the size of the 1D intervention space \mathcal{X} , so that the uniform intervention distribution $I_D(x) = 1/L$.

With these expressions, we can now calculate the $EI = \langle D_{KL}[P(y | x) \| E_D(y)] \rangle_{I_D(x)}$. Since σ is small, the Gaussian for $P(y | x)$ will ensure that θ_x is close to θ_y , and so to leading order we replace $\sigma(\theta_x, \theta_y) \approx \sigma(\theta_x, \theta_x)$ here. So:

$$EI = \int \frac{dx}{L} \int \underbrace{\frac{dy}{f'(\theta_y)}}_{=d\theta_y} \frac{1}{\sqrt{2\pi \sigma^2(\theta_x)}} e^{-\frac{(\theta_x - \theta_y)^2}{2\sigma^2(\theta_x)}} \left(-\frac{(\theta_x - \theta_y)^2}{2\sigma^2(\theta_x)} - \log \left[f'(\theta_y) \sqrt{2\pi \sigma^2(\theta_x)} \right] - \log \left[\frac{F'(\theta_y)}{L f'(\theta_y)} \right] \right)$$

$$= \int \frac{dx}{L} \left(-\frac{1}{2} - \log \left[f'(\theta_x) \sqrt{2\pi \sigma^2(\theta_x)} \right] - \log \left[\frac{F'(\theta_x)}{L f'(\theta_x)} \right] \right)$$

$$= -\frac{1}{2} \int \frac{d\theta F'(\theta)}{L} \log \left[2\pi e \left(\frac{F'(\theta)}{L} \right)^2 \left(\left(\frac{\epsilon}{f'(\theta)} \right)^2 + \left(\frac{\delta}{F'(\theta)} \right)^2 \right) \right] \quad (\text{A5})$$

$$= \log \left[\frac{L}{\delta \sqrt{2\pi e}} \right] - \frac{\delta}{L} \int d\theta \sqrt{h(\theta)} \log \sqrt{h(\theta) (h^{-1}(\theta) + g^{-1}(\theta))} \quad (\text{A6})$$

where in the last line we simply rearranged and substituted the expressions for the metrics $g(\theta)$ and $h(\theta)$ from Eq. A1. Here we first see that line A5 reproduces the EI approximation we showed for the dimmer switch example, in Eq. 4, for the setup there: $F(\theta) = \theta$, and $L = 1$. In general, by recognizing that here the volume of the intervention space is $V_I = \int d\theta \sqrt{h(\theta)} = \int d\theta F'(\theta) / \delta = L / \delta$, we finally see that expression in Eq. A6 agrees with our main result presented in Eq. 7 in the case of a 1D parameter space discussed here.

Appendix A.2. Multi-dimensional case

Generalizing the above derivation to multi-dimensional case is straightforward, and is mainly a matter of careful bookkeeping. The expressions in Eq. A1 become here:

$$\begin{aligned}
 &\text{interventions } x^a \in \mathcal{X}, \text{ parameters } \theta^\mu \in \Theta, \text{ effects } y^i \in \mathcal{Y} \\
 &x \rightarrow q(\theta | x), \quad \text{such that } \tilde{q}(x | \theta) \equiv \frac{q(\theta | x)}{\int d^d x q(\theta | x)} = \frac{\sqrt{\det \Delta_{ab}}}{(2\pi)^{d_I/2}} e^{-\frac{1}{2} \Delta_{ab} (x - F(\theta))^a (x - F(\theta))^b} \\
 &\theta \rightarrow p(y | \theta) = \frac{\sqrt{\det E_{ij}}}{(2\pi)^{d_E/2}} e^{-\frac{1}{2} E_{ij} (y - f(\theta))^i (y - f(\theta))^j} \\
 &g_{\mu\nu}(\theta) = E_{ij} \partial_\mu f^i(\theta) \partial_\nu f^j(\theta) \quad \text{effect metric} \\
 &h_{\mu\nu}(\theta) = \Delta_{ab} \partial_\mu F^a(\theta) \partial_\nu F^b(\theta) \quad \text{intervention metric}
 \end{aligned} \tag{A7}$$

Here $a, b \in \{1, \dots, d_I\}$ index the various dimension of the intervention space \mathcal{X} , $\mu, \nu \in \{1, \dots, d\}$ —for dimensions of the parameter space Θ , and $i, j \in \{1, \dots, d_E\}$ —the effects space \mathcal{Y} . As we are dealing with general multi-dimensional geometric constructs, in this section we are being careful to denote the contravariant vector components with upper indices, as in θ^μ , and covariant components with lower indices, as in $\partial_\mu \equiv \frac{\partial}{\partial \theta^\mu}$.

As in Eq. A2, A3 above, we can then compute the distribution over effects conditioned on interventions:

$$\begin{aligned}
 P(y | x) &= \frac{\sqrt{\det \Sigma_{\mu\nu}(\theta_x, \theta_y)}}{\det(\partial_\mu f^i(\theta_y)) (2\pi)^{d/2}} e^{-\frac{1}{2} \Sigma_{\mu\nu} (\theta_x - \theta_y)^\mu (\theta_x - \theta_y)^\nu} \\
 &\text{with } \Sigma^{-1}(\theta_x, \theta_y) \equiv g^{-1}(\theta_y) + h^{-1}(\theta_x)
 \end{aligned} \tag{A8}$$

where Σ denotes the matrix with components $\Sigma_{\mu\nu}$, and Σ^{-1} its matrix inverse (and similar for g and h). Here we assumed that both functions $F(\theta)$ and $f(\theta)$ are invertible, which means that the intervention and effect spaces \mathcal{X} and \mathcal{Y} both have the same dimension as the parameter space Θ : $d_I = d_E = d$. This allows us to view the map $\theta^\mu \rightarrow f^i(\theta)$ as a change of coordinates, with a square Jacobian matrix $\partial_\mu f^i$, whose determinant in the first line of Eq. A8 is thus well-defined, and may be usefully expressed as $\det(\partial_\mu f^i) = \sqrt{\frac{\det g_{\mu\nu}}{\det E_{ij}}}$. Note also that to get the above result, we once again assumed the distributions $\tilde{q}(x | \theta)$ and $p(y | \theta)$ to be nearly deterministic, meaning here that the matrices Δ and E must be large, though the precise form of the assumption is messy here.

Averaging this result over the intervention space \mathcal{X} , we get:

$$E_D(y) = \langle P(y | x) \rangle_{\mathcal{X}} = \frac{\det(\partial_\mu F^a(\theta_y))}{\det(\partial_\mu f^i(\theta_y))} \frac{\sqrt{\det \Delta_{ab}}}{V_I} \tag{A9}$$

where we defined intervention-space volume in units of variance of \tilde{q} , as: $V_I \equiv \int d^d x \sqrt{\det \Delta_{ab}} = \int d^d \theta \sqrt{\det h_{\mu\nu}(\theta)}$. Performing another such average over \mathcal{X} , with some algebra, similar as for Eq. A5, we can arrive at our result in Eq. 7:

$$EI = \langle D_{KL} [P(y | x) \| E_D(y)] \rangle_{\mathcal{X}} = \log \left[\frac{V_I}{(2\pi e)^{d/2}} \right] - \frac{1}{V_I} \int d^d \theta \sqrt{\det h} \log \sqrt{\det(\mathbb{1} + g^{-1} h)} \tag{A10}$$

References

1. Hoel, E.P. Agent above, atom below: how agents causally emerge from their underlying microphysics. In *Wandering Towards a Goal*; Springer, 2018; pp. 63–76.
2. Anderson, P.W. More is different. *Science* **1972**, *177*, 393–396.
3. Solé, R.V.; Manrubia Cuevas, S.; Luque, B.; Delgado, J.; Bascompte, J. Phase transitions and complex systems: Simple, nonlinear models capture complex systems at the edge of chaos **1996**.
4. Zenil, H.; Soler-Toscano, F.; Joosten, J.J. Empirical encounters with computational irreducibility and unpredictability. *Minds and Machines* **2012**, *22*, 149–165.
5. Israeli, N.; Goldenfeld, N. Computational irreducibility and the predictability of complex physical systems. *Physical review letters* **2004**, *92*, 074105.
6. Transtrum, M.K.; Machta, B.B.; Brown, K.S.; Daniels, B.C.; Myers, C.R.; Sethna, J.P. Perspective: Sloppiness and emergent theories in physics, biology, and beyond. *The Journal of chemical physics* **2015**, *143*, 07B201_1.
7. Box, G.E. Science and statistics. *Journal of the American Statistical Association* **1976**, *71*, 791–799.
8. Maiwald, T.; Hass, H.; Steiert, B.; Vanlier, J.; Engesser, R.; Raue, A.; Kipkeew, F.; Bock, H.H.; Kaschek, D.; Kreutz, C.; others. Driving the model to its limit: profile likelihood based model reduction. *PloS one* **2016**, *11*, e0162366.
9. MacKay, D.J.; Mac Kay, D.J. *Information theory, inference and learning algorithms*; Cambridge university press, 2003.
10. Amari, S.i. *Information geometry and its applications*; Vol. 194, Springer, 2016.
11. Gutenkunst, R.N.; Waterfall, J.J.; Casey, F.P.; Brown, K.S.; Myers, C.R.; Sethna, J.P. Universally sloppy parameter sensitivities in systems biology models. *PLoS computational biology* **2007**, *3*.
12. Transtrum, M.K.; Qiu, P. Model reduction by manifold boundaries. *Physical review letters* **2014**, *113*, 098701.
13. Mattingly, H.H.; Transtrum, M.K.; Abbott, M.C.; Machta, B.B. Maximizing the information learned from finite data selects a simple model. *Proceedings of the National Academy of Sciences* **2018**, *115*, 1760–1765.
14. Machta, B.B.; Chachra, R.; Transtrum, M.K.; Sethna, J.P. Parameter space compression underlies emergent theories and predictive models. *Science* **2013**, *342*, 604–607.
15. Raju, A.; Machta, B.B.; Sethna, J.P. Information loss under coarse graining: A geometric approach. *Physical Review E* **2018**, *98*, 052112.
16. Laughlin, R.B.; Pines, D. From the cover: The theory of everything. *Proceedings of the national academy of sciences of the United States of America* **2000**, *97*, 28.
17. Sugihara, G.; May, R.; Ye, H.; Hsieh, C.h.; Deyle, E.; Fogarty, M.; Munch, S. Detecting causality in complex ecosystems. *science* **2012**, *338*, 496–500.
18. Solvang, H.K.; Subbey, S. An improved methodology for quantifying causality in complex ecological systems. *PloS one* **2019**, *14*, e0208078.
19. Pearl, J. *Causality*; Cambridge university press, 2009.
20. Tononi, G.; Sporns, O. Measuring information integration. *BMC neuroscience* **2003**, *4*, 31.
21. Hoel, E.P.; Albantakis, L.; Tononi, G. Quantifying causal emergence shows that macro can beat micro. *Proceedings of the National Academy of Sciences* **2013**, *110*, 19790–19795.
22. Hoel, E.P. When the map is better than the territory. *Entropy* **2017**, *19*, 188.
23. Pearl, J.; Mackenzie, D. *The book of why: the new science of cause and effect*; Basic Books, 2018.
24. Balduzzi, D. Information, learning and falsification. *arXiv preprint arXiv:1110.3592* **2011**.
25. Klein, B.; Hoel, E. The emergence of informative higher scales in complex networks. *Complexity* **2020**, *2020*.
26. Liu, Y.Y.; Slotine, J.J.; Barabási, A.L. Controllability of complex networks. *nature* **2011**, *473*, 167–173.
27. Portugal, R.; Svaite, B.F. Weber-Fechner law and the optimality of the logarithmic scale. *Minds and Machines* **2011**, *21*, 73–81.
28. Hu, W.; Davis, W. Dimming curve based on the detectability and acceptability of illuminance differences. *Optics express* **2016**, *24*, A885–A897.
29. Dufresne, E.; Harrington, H.A.; Raman, D.V. The geometry of sloppiness. *arXiv preprint arXiv:1608.05679* **2016**.

30. Transtrum, M.K.; Machta, B.B.; Sethna, J.P. Geometry of nonlinear least squares with applications to sloppy models and optimization. *Physical Review E* **2011**, *83*, 036701.
31. Tikhonov, M. Theoretical ecology without species. *Bulletin of the American Physical Society* **2016**, *61*.
32. Blumer, A.; Ehrenfeucht, A.; Haussler, D.; Warmuth, M.K. Occam's razor. *Information processing letters* **1987**, *24*, 377–380.
33. Shapiro, L. *Embodied cognition*; Routledge, 2019.
34. Srednicki, M. *Quantum field theory*; Cambridge University Press, 2007.